RSC Advances

ROYAL SOCIETY OF CHEMISTRY

www.rsc.org/advances

A Table of Contents Entry

Sol-gel Synthesis and Electrochemical Properties of c-Axis Oriented $LiCoO_2$ for Lithium-ion Batteries

Sen Gao,[a] Wei Wei,[a] Maixia Ma,[a] Juanjuan Qi,[a] Jie Yang,[a] Shengqi Chu,[b] Jing Zhang[b] and Lin Guo[*a]*

This paper expounds the relationship between electrochemical performance and degree of c-axis orientation of $LiCoO_2$.

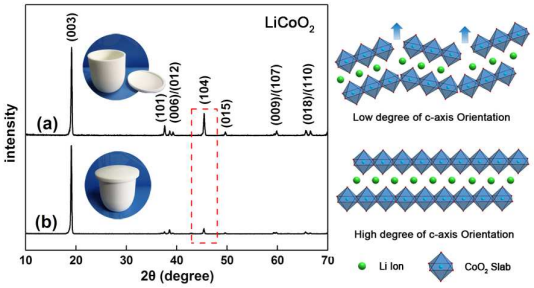

RSC Advances

ARTICLE

Sol-gel Synthesis and Electrochemical Properties of c-Axis Oriented $LiCoO_2$ for Lithium-ion Batteries†

Received 00th January 20xx,
Accepted 00th January 20xx

DOI: 10.1039/x0xx00000x

www.rsc.org/

Sen Gao,[a] Wei Wei,[a] Maixia Ma,[a] Juanjuan Qi,[a] Jie Yang,[a] Shengqi Chu,[b] Jing Zhang[b] and Lin Guo*[a]

For better performance of $LiCoO_2$ as cathode for lithium-ion batteries, electrochemical properties of c-axis oriented $LiCoO_2$ were studied. $LiCoO_2$ with controllable intensity ratios of peak (003) to peak (104) were synthesized via a resorcinol-formaldehyde sol-gel method, followed by an air-controlled high temperature treatment. Electrochemical measurements show that $LiCoO_2$ with low degree of c-axis orientation exhibited a better performance than $LiCoO_2$ with high degree of c-axis orientation. X-ray absorption spectroscopy was used to reveal the texture-property relationship between different products. The variances could be attributed to different electrochemical active sites created and diffusion lengths for lithium ions related to c-axis orientation.

Introduction

As a solution to the worldwide energy crisis, lithium ion batteries (LIB) technology has been well developed and widely used for the portable electronic devices in the past twenty years. However, performance requirements are raised for LIB to be applied in the high-power transportation system, such as the hybrid electric vehicles (HEVs) or electric vehicles (EVs).[1,2] In current LIB technology, the capacity as well as Li^+ transportation is mainly determined by the cathode material, which makes the developments of cathode materials extremely crucial.[3,4] $LiCoO_2$ was the first commercially successful cathode for LIB and still occupies more than 90% of the cathode material market today.[2] To improve the performance of $LiCoO_2$, besides transition metal doping,[5] new structure design[6-8] proves to be an effective way in recent years. Crystalline $LiCoO_2$ adopts the layered α-$NaFeO_2$-type structure (space group R-3m) with lithium and cobalt ions ordered in the octahedral sites of alternating (111) planes, which can be typically described by a hexagonal unit cell with a_{hex}=2.816 Å and c_{hex}=14.08 Å.[9] Electrochemical lithium insertion/removal behaviour of the layered $LiCoO_2$ strongly depends on the orientations of the crystal due to its anisotropic crystallographic structure.[10,11] $LiCoO_2$ is apt to crystallize with c-axis orientation since the (003) plane has the lowest surface energy with the highest atomic density of all planes.[12-14] Thus, it is critical to investigate the effect of c-axis orientation on electrochemical performance of $LiCoO_2$.

By far, the reports of the c-axis oriented $LiCoO_2$ mainly focus on the $LiCoO_2$ thin film electrodes for all-solid-state lithium microbatteries.[10,13-15] Considering of $LiCoO_2$ composite powder electrodes, some early studies[16,17] reported c-axis oriented $LiCoO_2$ crystals preferentially dominated by (003) planes, and explained that stronger (003) intensity led to lower degree of cation disorder. Since cation mixing is more likely to occur in $LiNiO_2$,[18] $LiNi_{0.5}Mn_{0.5}O_2$,[19,20] and Li-Co-Ni-Mn-O layered compound,[21,22] more evidence is needed to confirm the hypothesis above. Recently, there were also reports such as $LiCoO_2$ nanoplates[4] and micro-sized flake-like $LiCoO_2$ particles[23] with preferentially exposed (001) planes. However, the effect of the degree of c-axis orientation on electrochemical behaviour and in $LiCoO_2$ has not been investigated yet.

In the present work, we synthesized $LiCoO_2$ with different degrees of c-axis orientation via a facile resorcinol-formaldehyde (RF) sol-gel method,[24-26] followed by an air-controlled calcination process. Then X-ray absorption fine structure (XAFS) technique, including X-ray absorption near-edge structure (XANES) and extended X-ray absorption fine structure (EXAFS), was firstly used to reveal the texture-property relationship of c-axis oriented $LiCoO_2$ cathode materials, and the effect of the degree of texture on the electrochemical performance of the as-prepared products was discussed.

Experimental

Preparation of Materials

In a typical synthesis, 0.005 mol $Co(CH_3COO)_2{\cdot}4H_2O$ and $LiCH_3COO{\cdot}2H_2O$ containing a 5 mol% excess of Li were dissolved into 25 ml of anhydrous alcohol, which included 0.025 mol resorcinol and 0.05 mol formaldehyde (38.5 % in water, methanol stabilized), yielding a light pink suspension. After 3 h of vigorous agitation at room temperature, the homogeneous mixture solution was heated to 60 °C in a water

[a] School of Chemistry and Environment, Beihang University, Beijing 100191, P. R. China. Email: guolin@buaa.edu.cn
[b] Institute of High Energy Physics, the Chinese Academy of Sciences, Beijing, 100049, P. R. China.

† Electronic Supplementary Information (ESI) available. See DOI: 10.1039/x0xx00000x

bath under magnetic stirring until viscous, and then dried completely in an electric oven at 90 °C. Finally, the gels were placed in alumina crucibles (30 ml, Al_2O_3 ≥ 95 %) and calcined at 900 °C for 2 h in a muffle furnace (Zhonghuan, China) both covered and uncovered in air to obtain fine powders. All chemical reagents used in this experiment were of analytical grade and used without further purification.

Characterization of Materials

The phases and structures of the as-prepared products were characterized by X-ray powder diffraction (XRD) using a Rigaku Dmax2200 X-ray diffractometer with Cu Kα radiation (λ = 1.5406 Å) at 40 kV and 40 mA. Data were recorded in the range of 10° to 70° with a scan rate of 6° min^{-1}. Morphological studies were conducted using a field-emission gun environmental scanning electron microscope (Quanta 250 FEG). Elemental maps (Fig. S3 and S4, ESI†) were obtained by energy dispersive X-ray spectroscopy (FESEM/EDS, JSM-7500F). Transmission electron microscopy (TEM) study was performed by a JEOL JEM-2100F microscope. The Co K-edge X-ray absorption fine structure (XAFS) spectroscopy was measured at the 1W1B-XAFS beam line in Beijing Synchrotron Radiation Facility (BSRF), China. The storage ring of BSRF was operated at 2.5 GeV with a maximum current of 200 mA. A Si (111) double-crystal monochromator was used to monochromatize the radiation. The XAFS signals were collected in transmission mode at room temperature. XAFS spectra were analyzed by Athena and Artemis from ifeffit 1.2.11 software package,[27] which was then fitted in R-space with theoretical models based on the crystal structure of $LiCoO_2$ by FEFF6.[28] The k values used to fit the Co K-edge EXAFS ranged from 2 to 14.35 $Å^{-1}$ to minimize noise.

Electrode Fabrication and Electrochemical Tests

The working electrodes were prepared by mixing 80 wt % active material, 10 wt % acetylene black, and 10 wt % polyvinylidene fluoride (PVDF). The mixture was then dissolved in N-methyl-2-pyrrolidinone (NMP), coated on pure aluminum disks (14 mm in diameter) and dried at 120 °C for 10 h. The working electrodes were compressed at 3 MPa before assembly. Electrochemical measurements were carried out via CR2032 type coin cells with metallic lithium as the counter/reference electrode, Celgard 2325 as separator, and a solution of 1M $LiPF_6$ dissolved in a mixture of ethylene carbonate (EC), dimethyl carbonate (DMC), ethyl methyl carbonate (EMC) (1:1:1, v/v/v) as electrolyte. The cells were then assembled in an argon-filled glove box (Dellix, China). The galvanostatic discharge-charge tests were performed on a Land CT2001A battery testing system (Jinnuo, China) at specific current densities from 3.0 to 4.2 V (vs. Li/Li^+) at room temperature. The electrochemical impedance measurements were conducted on a CHI660D electrochemical workstation (Chenhua, China) at an AC voltage of 5 mV amplitude in the range of 100 kHz-0.01 Hz.

Results and Discussion

Fig. 1 shows the powder XRD patterns of products prepared in covered and uncovered crucibles, respectively. The patterns

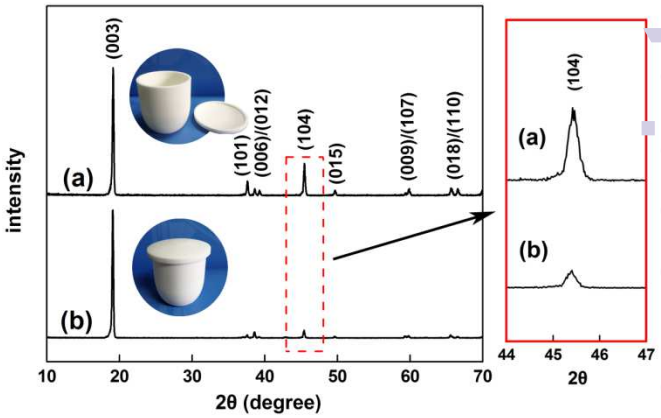

Fig. 1 XRD patterns of $LiCoO_2$ prepared in (a) covered and (b) uncovered crucibles.

can be indexed to the standard pattern of $LiCoO_2$ (PDF card No.75-0532). Both $LiCoO_2$ samples show a remarkably strong peak (003) and a relatively weak peak (104), indicating a preferred c-axis orientation (texture). The intensity ratios of (003) peak to (104) peak (I_{003}/I_{104}), which could be used as an indication of the degree of c-axis orientation,[17] are 4.0 and 16.5. Hereafter, $LiCoO_2$ with I_{003}/I_{104} values 4.0 and 16.5 are denoted as l-LCO ($LiCoO_2$ with low degree of c-axis orientation) and h-LCO ($LiCoO_2$ with high degree of c-axis orientation), respectively. A controlled experiment was conducted to show how the degree of c-axis orientation could be adjusted by such a simple method (Fig. S1, ESI†). It appeared that $LiCoO_2$ prepared in covered crucibles shown a much higher degree of the c-axis orientation.

Fig. 2 shows the SEM images of both l-LCO and h-LCO. The l-LCO is composed of several individual irregular particles (blue dashed line) that fused together (Fig. 2a). Apparently, the whole polycrystalline particles are kind of fragmental since the texture of each part varies. On the contrary, the gains are intact in h-LCO with clear laminar morphology (yellow dashed line, Fig. 2b). Layered structure could be clearly observed in

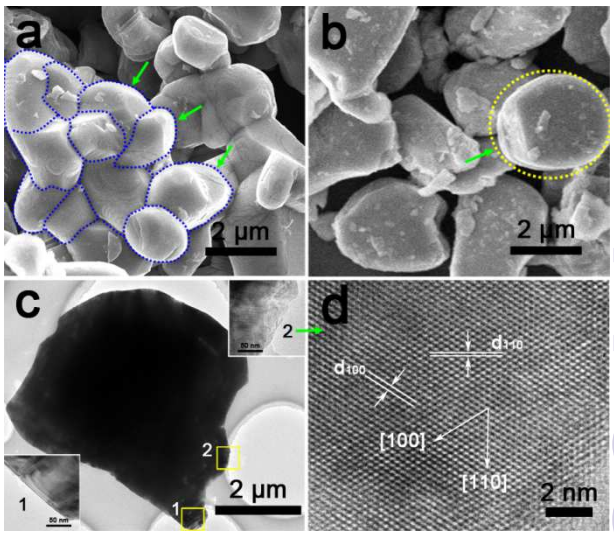

Fig. 2 SEM images of (a) the l-LCO and (b) the h-LCO; (c) TEM images of an individual h-LCO particle; (d) HRTEM images of inset No.2 in (c).

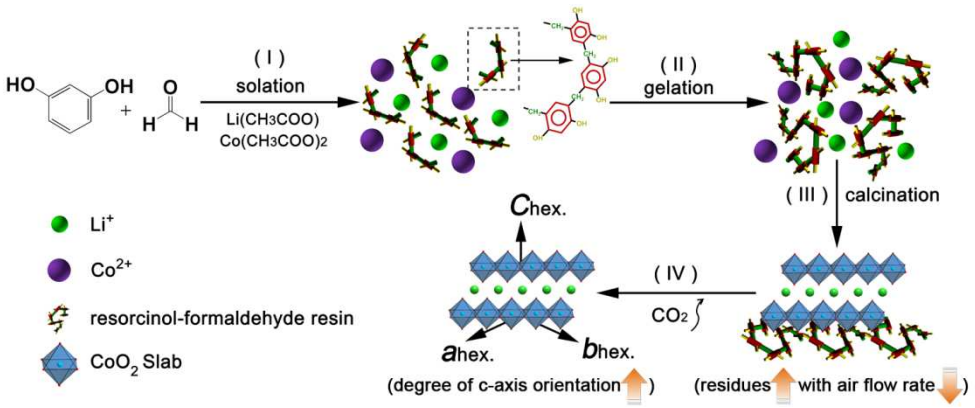

Fig. 3 Schematic illustration for the formation process of $LiCoO_2$ with different degrees of c-axis orientation.

inset No.1 of Fig. 2c. The frontal plane could be the (003) plane. In Fig. 2d, the frontal plane is confirmed as (003) plane, which is perpendicular to both the set of (110) planes with a crossing lattice interdistance of 0.14 nm and the set of (100) planes with a lattice interdistance of 0.25 nm.[12] The morphological analysis was in good agreement with the XRD results that h-LCO shown a higher I_{003}/I_{104} value than l-LCO.

The difference in degree of c-axis orientation could possibly be attributed to controlled air flow rates during heat treatment. It is generally accepted that the equilibrium form of a crystal tends to possess a minimal total surface energy.[29] During the calcination, the driving force of the atomic movement derived from the tendency of minimizing the surface energy. As shown in Fig. 3, with the crucible covered (with only a tiny gap to let air through), the flow rate of air w dramatically reduced, which caused a large amount of carbonaceous residues left due to the incomplete combustion of the RF resin. After that, these residues served as nucleation centers for $LiCoO_2$ during the calcination and finally completely transformed to volatile products. $LiCoO_2$ crystallized on the surface of residues and facilitated the formation of grains with exposed (003) planes, which are quite stable with the lowest surface energy.[12-14] In this way, h-LCO exposing (003) planes was obtained. Conversely, l-LCO was prepared with little help of residue nucleation centers during calcination process when the crucible was uncovered.

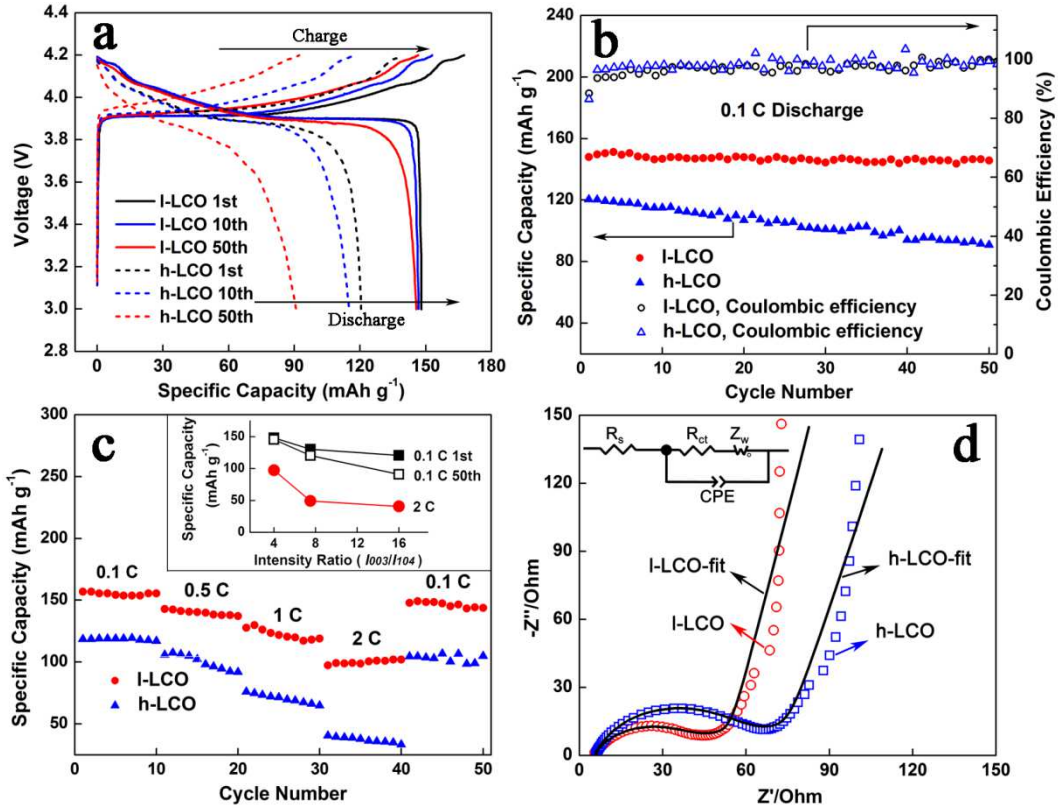

Fig. 4 (a) The charge/discharge curves at the 1st, 10th and 50th cycles for l-LCO and h-LCO; (b) Cycling performances and coulombic efficiency for l-LCO and h-LCO at 0.1 C; (c) R ce capacities of l-LCO and h-LCO at different rates stepwise from 0.1 to 2C (inset: specific capacity vs. intensity ratio I_{003}/I_{104}); (d) the impedance spectra (both experimental data a fitted curves) of l-LCO and h-LCO (inset: equivalent circuit used in fitting the impedance data, R_s, series resistance; R_{ct}, charge-transfer resistance; Z_w, Warburg impedance; CP constant phase element).

Then, the electrochemical performances of both products were measured (Fig. 4). Fig. 4a shows typical charge/discharge curves at the 1st, 10th and 50th cycles, measured at a current rate of 0.1 C in the range of 3.0-4.2 V. The initial discharge capacities of l-LCO and h-LCO at 0.1 C are 148.1 and 120.5 mA $h \cdot g^{-1}$. After 50 cycles, the discharge capacities remain 145.7 and 90.8 mA $h \cdot g^{-1}$ (corresponding to capacity retentions of 98.4% and 75.4%), respectively. It seemed that the reversible capacity of h-LCO faded faster than l-LCO. Fig. 4b shows the cycling performances and coulombic efficiency for l-LCO and h-LCO. The coulombic efficiencies at the first cycle are relatively low for l-LCO (88.4%) and h-LCO (86.6%), which could be attributed to the large charge capacity during the formation of solid electrolyte interphase (SEI) layer.[30] The average coulombic efficiency of l-LCO from the 2rd to the 50th cycle is 97.2%, a little lower than that of h-LCO (98.4%). Fig. 4c illustrates the discharge curves at different rates. The l-LCO and h-LCO deliver rate capacities of 97.4 and 40.5 mA $h \cdot g^{-1}$ at 2C, which means 62.1% and 34.1% of the capacities at 0.1C are retained. The inset in Fig. 4c shows the electrochemical performances of l-LCO, m-LCO ($LiCoO_2$ with medium degree of c-axis orientation, Fig. S2, ESI†) and h-LCO, as a function of the I_{003}/I_{104} value. Clearly, both cycling and rate performances degrade with the increase o the I_{003}/I_{104} value, i.e. the degree of c-axis orientation. The impedance spectra of the materials are shown in Fig. 4d, consisting of a semicircle (charge-transfer resistance) and an inclined line (Warburg impedance).[31] The result of the fitting fits well with the experimental data. The charge-transfer resistance R_{ct} of h-LCO is 54 Ω, higher than that of l-LCO (38 Ω). As shown above, it turned out that $LiCoO_2$ with low degree of c-axis orientation exhibited a better electrochemical performance than that with high degree of c-axis orientation.

X-ray absorption fine structure (XAFS) spectra were performed to reveal the structure-performance relationship since they can provide information on the local environment around the center atoms.[32-35] Fig. 5a shows the normalized XANES spectra at Co K-edge of l-LCO and h-LCO with three characteristic peaks A, B and C. The pre-edge absorption peak A corresponds to the electric dipole-forbidden transition of the 1s electron to the unoccupied 3d orbital in Co^{3+}. The B and C peaks represent the dipole-allowed 1s to 4p transition with and without a shakedown process that originate from a ligand to metal charge transfer.[36,37] The difference in the position of peak C between these products is negligible, which indicates that there is no difference in cobalt oxidation state, and cobalt is located in octahedral sites.[38]

Fourier transforms (FTs) of Co K-edge k^3-weighted EXAFS spectra of l-LCO and h-LCO are demonstrated in Fig. 5b. The FT peaks at around 1.9 Å and 2.8 Å correspond to single scattering contributions from the nearest O atoms and Co atoms.[35,36] Comparing with Cobalt, the contribution of lithium coordination shell can be hardly seen due to the small scattering factor of the Li atom. As listed in Table 1, structural parameters of interatomic distances R and Debye-Waller factors σ^2 for the first two coordination shells are obtained from nonlinear least squares fitting. The Debye-Waller factor

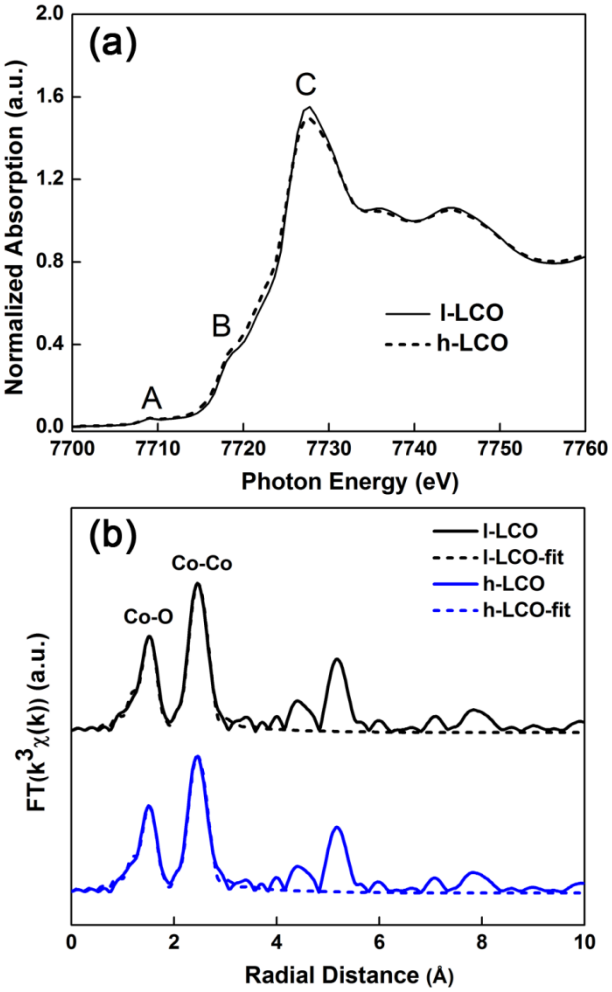

Fig. 5 (a) The normalized XANES spectra at Co K-edge of l-LCO and h-LCO; (b) Fourier transforms of Co K-edge k^3-weighted EXAFS spectra of l-LCO and h-LCO, shown with both Experimental and fitting curves.

σ^2 corresponds to the mean square relative atomic displacement of interatomic distance R for each bonding pair due to local disorder. The bondlength R of both Co-O and Co-Co shells in h-LCO are a little shorter than l-LCO, which is indicative that there is a little structural contraction in h-LCO without significant changes in R-3m structure.[38] The Debye-Waller factors for the l-LCO (σ^2 = 0.00337 $Å^2$ and 0.00301 $Å^2$ for Co-Co and Co-O) are larger than h-LCO (σ^2 = 0.00312 $Å^2$ and 0.00271 $Å^2$ for Co-Co and Co-O), consistent with larger

Table 1. Structural parameters of the curve fitting results for Co K-edge EXAFS.

Sample	Shell	N	R (Å)	σ^2 ($Å^2$)
l-LCO	Co-O	6	1.922	0.00337
	Co-Co	6	2.820	0.00301
h-LCO	Co-O	6	1.920	0.00312
	Co-Co	6	2.817	0.00271

N is the coordination number; R is the interatomic distance; σ^2 is the Debye-Waller factor.

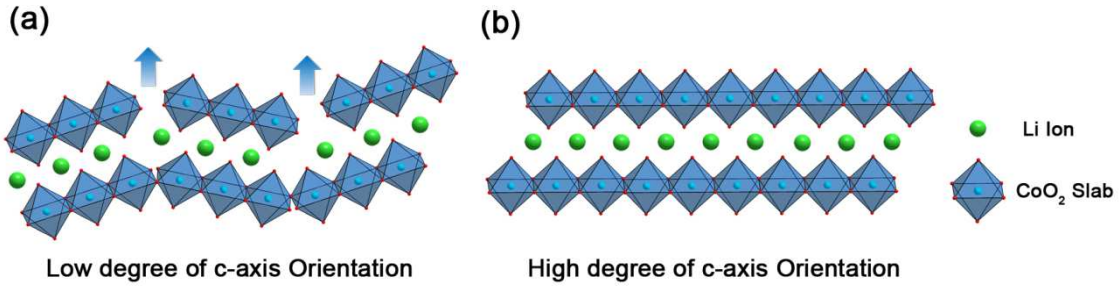

Fig. 6 Schematic illustration of lithium ions diffusion in $LiCoO_2$ with (a) low and (b) high degrees of c-axis orientation

disorder[35] in $LiCoO_2$ with low degree of c-axis orientation.

Combined with scanning electron microscope morphology analysis (Fig. 2), the CoO_2-sheets in h-LCO are considered to be intact and ordered, while distorted and fragmental in l-LCO. These differences in structure would possibly have significant impact on the electrochemical properties of $LiCoO_2$ as cathode material for Li-ion batteries. As illustrated in Fig. 6, with a large amount of O^{2-} and Co^{3+} ions blocking the pathway, Li ions can only move in two-dimensional directions between the CoO_2 slabs.[4,10,13,39] In addition, the diffusion time of Li^+ in $LiCoO_2$ is proportional to the square of the diffusion length.[40,41] With fragmental CoO_2-sheets, l-LCO (Fig. 6a) provides more electrochemical active sites and shorter diffusion channels for Li^+ to migrate during the insertion/removal process than h-LCO (Fig. 6b). The lower charge-transfer resistance R_{ct} could be attributed to the anisotropy in electron conductivity, which is much better along a-b-axis than c-axis.[11] Thus, the fact that l-LCO presents relatively better electrochemical performance, including better rate performance and cyclability than h-LCO could possibly be explained. On the other hand, the higher average coulombic efficiency of h-LCO may indicate that the reversibility is better between well-ordered CoO_2 sheets.

Conclusions

We investigated $LiCoO_2$ with different degrees of c-axis orientation to analyse the relationship between the texture and electrochemical properties in composite electrodes. $LiCoO_2$ with different I_{003}/I_{104} ratios were prepared via a sol-gel method followed by an air-controlled high temperature treatment. Electrochemical measurements shown that $LiCoO_2$ with low degree of texture exhibited a better performance: the l-LCO and h-LCO exhibited rate capacities of 97.4 and 40.5 mA $h \cdot g^{-1}$ at 2C, corresponding to capacity retentions of 62.1% and 34.1% comparing to 0.1C, respectively. As confirmed by crystallographic structures analysis and XAFS results, $LiCoO_2$ with low degree of c-axis orientation creates more electrochemical active sites and shorter diffusion distances for lithium ions, which is favourable for the electrochemical performance of $LiCoO_2$. Also, it can be known that high degree of c-axis orientation could possibly indicate particles with intact layered structure. To achieve better performance, oriented growth control would be an important strategy in the structure design of layered electrode materials.

Acknowledgements

This work was financially supported by the National Basic Research Program of China (2013CB934004) and the National Natural Science Foundation of China (11079002).

Notes and references

1 Y. X. Tang, Y. Y. Zhang, J. Y. Deng, D. P. Qi, W. R. Leow, J. Q. Wei, S. Y. Yin, Z. L. Dong, R. Yazami, Z. Chen and X. D. Chen, *Angew. Chem. Int. Ed.*, 2014, **53**, 13488-13492.
2 X. L. Xiao, X. F. Liu, L. Wang, H. Zhao, Z. B. Hu, X. M. He and Y. D. Li, *Nano Res.,* 2012, **5**, 395-401.
3 J. H. Yan, X. B. Liu and B. Y. Li, *RSC Adv.*, 2014, **4**, 63268.
4 B. Xu, D. Qian, Z. Y. Wang and Y. S. Meng, *Mater. Sci. Eng., R,* 2012, **73**, 51-65.
5 J. Liang, D. H. Wu, M. Hu, Y. Tian, J. P. Wei and Z. Zhou, *Electrochim. Acta*, 2014, **146**, 784-791.
6 M. Okubo, E. Hosono, J. Kim, M. Enomoto, N. Kojima, T. Kudo, H. S. Zhou and I. Honma, *J. Am. Chem. Soc.,* 2007, **129**, 7444-7452.
7 H. L. Chen and C. P. Grey, *Adv. Mater.,* 2008, **20**, 2206-2210.
8 D. S. Wang, X. L. Ma, Y. G. Wang, L. Wang, Z. Y. Wang, W. Zheng, X. M. He, J. Li, Q. Peng and Y. D. Li, *Nano Res.,* 2010, **3**, 1-7.
9 K. Mizushima, P. C. Jones, P. J. Wiseman and J. B. Goodenough, *Mater. Res. Bull.,* 1980, **15**, 783-789.
10 Y. Iriyama, M. Inaba, T. Abe and Z. Ogumi, *J. Power Sources,* 2001, **94**, 175-182.
11 H. T. Zhang, P. J. Baker and P. S. Grant, *J. Am. Ceram. Soc.,* 2010, **93**, 1856-1859.
12 G. Z. Wei, X. Lu, F. S. Ke, L. Huang, J. T. Li, Z. X. Wang, Z. Y. Zhou and S. G. Sun, *Adv. Mater.,* 2010, **22**, 4364-4367.
13 J. B. Bates, N. J. Dudney, B. J. Neudecker, F. X. Hart, H. P. Jun and S. A. Hackney, *J. Electrochem. Soc.,* 2000, **147**, 59-70.
14 Y. Yoon, C. Park, J. Kim and D. Shin, *J. Power Sources,* 2013, **226**, 186-190.
15 J. Xie, N. Imanishi, T. Matsumura, A. Hirano, Y. Takeda and O. Yamamoto, *Solid State Ionics,* **2008**, *179*, 362-370.
16 M. Yoshio, H. Tanaka, K. Tominaga and H. Noguchi, *J. Power Sources,* 1992, **40**, 347-353.
17 W. P. Tang, H. Kanoh and K. Ooi, *Electrochem. Solid-State Lett.,* 1998, **1**, 145-146.
18 T. Ohzuku, A. Ueda, M. Nagayama, Y. Iwakoshi and H. Komori, *Electrochim. Acta,* 1993, **38**, 1159-1167.
19 J. Bréger, N. Dupré, P. J. Chupas, P. L. Lee, T. Proffen, J. B. Parise and C. P. Grey, *J. Am. Chem. Soc.,* 2005, **127**, 7529-7537.
20 J. Bréger, Y. S. Meng, Y. Hinuma, S. Kumar, K. Kang, Y. Shao-Horn, G. Ceder and C. P. Grey, *Chem. Mater.,* 2006, **18**, 4768-4781.

21 C. H. Lei, J. Bareño, J. G. Wen, I. Petrov, S. H. Kang and D. P. Abraham, *J. Power Sources,* 2008, **178**, 422-433.
22 B. Xu, C. R. Fell, M. F. Chi and Y. S. Meng, *Energy Environ. Sci.,* 2011, **4**, 2223-2233.
23 T. Wei, R. Zeng, Y. M. Sun, Y. H. Huang and K. Huang, *Chem. Commun.,* 2014, **50**, 1962-1964.
24 K. M. Shaju and Peter G. Bruce, *Adv. Mater.*, 2006, **18**, 2330-2334.
25 H. M. Yang, X. J. Cui, Y. Q. Deng and F. Shi, *RSC Adv.*, 2014, **4**, 59754.
26 Y. Kong, X. Shen, S. Cui and M. H. Fan, *RSC Adv.*, 2014, **4**, 64193.
27 B. Ravel and M. Newville, *J. Synchrotron Rad.,* 2005, **12**, 537-541.
28 S. I. Zabinsky, J. J. Rehr, A. Ankudinov, R. C. Albers and M. J. Eller, *Phys. Rev. B,* 1995, **52**, 2995-3009.
29 A. F. Wells, *Structural Inorganic Chemistry,* 5th ed.; Clarendon Press: Oxford, 1984.
30 B. R. Wu, Y. H. Ren, D. B. Mu, X. J. Liu, G. C. Yang and F. Wu, *RSC Adv.*, 2014, **4**, 10196.
31 Y. Mizuno, E. Hosono, T. Saito, M. Okubo, D. Nishio-Hamane, K. Oh-ishi, T. Kudo and H. S. Zhou, *J. Phys. Chem. C*, 2012, **116**, 10774-10780.
32 J. Bareño, M. Balasubramanian, S. H. Kang, J. G. Wen, C. H. Lei, S. V. Pol, I. Petrov and D. P. Abraham, *Chem. Mater.*, 2011, **23**, 2039-2050.
33 S. Permien, H. Hain, M. Scheuermann, S. Mangold, V. Mereacre, A. K. Powell, S. Indris, U. Schürmann, L. Kienle, V. Duppel, S. Harm and W. Bensch, *RSC Adv.*, 2013, **3**, 23001.
34 L. Simonelli, N. L. Saini, M. M. Sala, M. Okubo, I. Honma, T. Mizokawa, G. Monaco, *Appl. Phys. Lett.,* 2013, **103**, 083111.
35 L. Maugeri, L. Simonelli, A. Iadecola, B. Joseph, M. Okubo, I. Honma, H. Wadati, T. Mizokawa and N. L. Saini, *J. Power Sources,* 2013, **229**, 272-276.
36 T. Nedoseykina, S. S. Kim and Y. Nitta, *Electrochim. Acta,* 2006, **52**, 1467-1471.
37 T. Okumura, Y. Yamaguchi, M. Shikano and H. Kobayashi, *J. Mater. Chem.,* 2012, **22**, 17340-17348.
38 A. V. Chadwick, S. L. P. Savin, R. Alcántara, D. F. Lisbona, P. Lavela, G. F. Ortiz and J. L. Tirado, *ChemPhysChem,* 2006, **7**, 1086-1091.
39 S. I. Zabinsky, J. J. Rehr, A. Ankudinov, R. C. Albers and M. J. Eller, *Phys. Rev. B,* 1995, **52**, 2995-3009.
40 P. G. Bruce, B. Scrosati and J. M. Tarascon, *Angew. Chem. Int. Ed.,* 2008, **47**, 2930-2946.
41 H. J. Zhang, C. C. Wong and Y. Wang, *Cryst. Growth Des.,* 2012, **12,** 5629-5634.